Research on the effect of solution acidity and alkalinity on microstructure and properties of tungsten alloys reinforced by yttria stabilized zirconia particles

Fangnao Xiao [a, c], Thierry Barriere [a], Gang Cheng [b], Qiang Miao [c*], Shizhong Wei [d*], Liujie Xu [d*]

[a] Univ. Bourgogne Franche-Comté, FEMTO-ST Institute, CNRS/UFC/ENSMM/UTBM, Department of Applied Mechanics, 25000 Besançon, France;

[b] INSA CVL, Univ. Tours, Univ. Orléans, LaMé, 3 rue de la Chocolaterie, BP 3410, 41034 Blois Cedex, France;

[c] College of Material Science and Technology, Nanjing University of Aeronautics and Astronautics, 29 Yudao Street, Nanjing 210000, China;

[d] National Joint Engineering Research Center for abrasion control and molding of metal materials, Henan University of Science and Technology, Luoyang 471003, China;

**Abstract:** Yttria stabilized zirconia particles [$Zr(Y)O_2$] strengthened tungsten alloys [W-$Zr(Y)O_2$] was developed via azeotropic distillation method combined with powder metallurgy method. The effects of acidity and alkalinity of original solution on the precursor powders' morphology, alloys' microstructure and properties were investigated deeply. The results show that precursor powders synthesized under solution with pH=2 possesses finer particles. The grain sizes of W-$Zr(Y)O_2$ alloys prepared under different pH values are almost same in range of 2-6 μm, much smaller than that of pure tungsten. As pH value increased from 2 to 8, there are more and more bonding $Zr(Y)O_2$ particles observed. W-$Zr(Y)O_2$ alloy prepared under pH=2 possesses better microstructure and compressive properties compared to other two alloys prepared under pH=5 and pH=8, respectively. The wear resistance increased firstly and then decreased with increasing $Zr(Y)O_2$ mass fraction. The optimal amount of $ZrO_2$ for improving wear property is 3%.

**Keywords:** Tungsten alloy; Zirconia doping; Yttria stabilized; Compressive strength.

## 1.Introduction

Tungsten alloys have been very widely used in the defense industry, nuclear reactor, and space vehicle equipment, because of its high melting point, high hardness, high strength at room and high temperature [1, 2]. Especially, the researches on the oxide dispersion-strengthened tungsten (ODS-W) have attracted considerable attentions [3], as these stable oxide particles were expected to decrease the high ductile-brittle transition temperature and enhance recrystallization temperature [4].

In the past several years, lots of liquid-liquid methods were introduced to prepare the ODS-W alloys [5, 6]. However, previous researches mainly focus on the research on the mechanical properties, such as bending strength, tensile strength and torsional fatigue strength and so on [7]. There are limited researches concerning the effect of liquid-liquid methods on precursor powders and microstructure of alloy. Actually, as reported in our previous research [5, 7], the morphology and composition of precursor affect greatly the morphology and distribution of oxide particle in reduced powders, which further affect the tungsten grain size, eventual oxide particle size and distribution. It is reported [8] that solutions with different acidities have a great effect on the reduced tungsten powders. However, the researches concerning the effect of solution acidity and alkalinity on precursor powders, microstructure and properties of tungsten alloys haven't been reported in detail.

In present research, the precursor powders and alloys under different pH values of 2, 5 and 8 (denoted as pH2, pH5 and pH8 powder/alloys below), were compared. Moreover, the microstructure, mechanical properties and abrasion resistance of alloys prepared under different pH values were investigated.

## 2. Experimental procedure

### 2.1 Chemical composition and preparation of alloys

In this research, tungsten alloys were developed via the azeotropic distillation method combined with the powder metallurgy method. The compositions of W-3wt%Zr(Y)$O_2$ and the azeotropic distillation process were reported elsewhere [8 ,9]. The synthesized precursor powders were calcined, followed by two reduction processes 750℃ × 2 h + 900℃ × 4 h in a hydrogen atmosphere to obtain W-Zr(Y)$O_2$ powders.

The W-Zr(Y)$O_2$ powders were pressed into a rubber mold at 350 MPa pressure for 30 min using a cold isostatic press to obtain cylindrical billets of Φ20 mm × 30 mm. The samples were then placed into a medium-frequency induction sintering furnace under a hydrogen atmosphere ($H_2$). The pre-sintering temperature was 1250°C for 2 h and the sintering temperature was 2400°C for 4 h. Finally, the W-Zr(Y)$O_2$ alloys were prepared.

**2.2 Measurement and analysis**

Compression test was carried out at room temperature using a universal material machine (AG-I250KN) with 1.0 mm/min speed of compression. The wear properties of the alloys were studied using a pin-on-dish (ML-100 type) friction testing machine with different grit alumina waterproof-abrasive sand papers of 240#, 360#, 600# and 800#, respectively, under the load of 40 N. The diagram of the ML-100-type wear tester was shown in reference [9]. The friction testing process was described elsewhere in detail [6]. The dimensions of the samples are Φ6 mm × 20 mm. Each sample moved repeatedly for 20 times. The samples were weighed using a digital micrometer with a least count of 0.1 mg. For each tungsten alloy, three samples were selected, and the wear weight loss for each sample was an average result of the three repetitions.

The morphology, microstructure and chemical composition of powders and alloy were observed through a scanning electron microscope (SEM) and backscatter electron image (BSE). High-resolution transmission electron microscopy (HR-TEM) was employed to observe the microstructure.

**3 Analysis and results**

**3.1 Analysis of precursor powders synthesized under different pH values**

Fig.1 shows the SEM images of precursor powders synthesized through azeotropic distillation method under different pH values. Seen from in Fig. 1a, as the pH value of the solution increases, the particle size increases and the morphology changes greatly. In Fig. 1a, the particles possess granular structure with a size of about 1 μm, while a small number of particles are plate-like structure [9]. When the pH of the solution is 5, the morphology of the precursor powder is mainly plate-shaped and block-shaped. The length of the plate-shaped particle is less than 10 μm, the particle surface is smooth and the dispersion is good. As can be seen from Fig. 1c, when the pH of the solution is 8, the particles mainly show a blocky structure with a particle size of 1-10 μm. According to the analysis above, pH value of solution affects significantly the morphology, this is due to that different polytungstate species exist in solutions resulted from different pH values. In our previous research [8], the reaction mechanism between polytungstate species with $H^+$/ $OH^-$ had been discussed in detail.

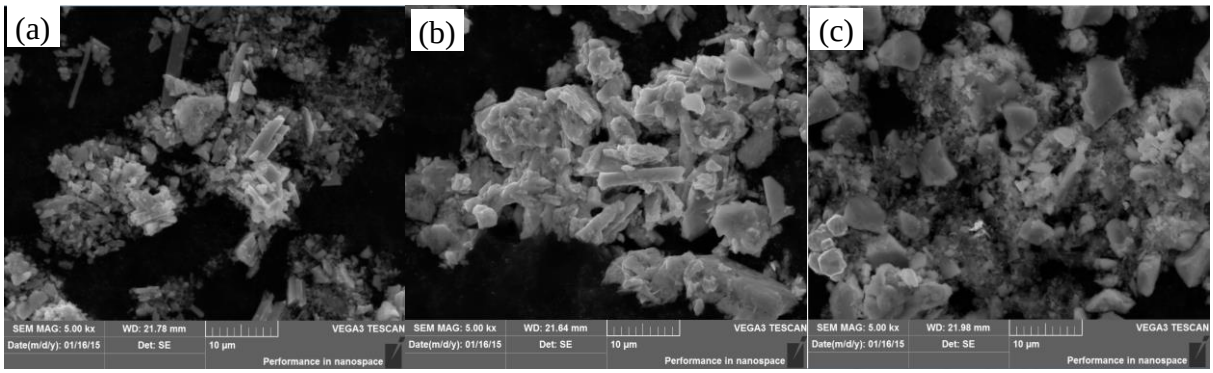

Fig.1 SEM images of the precursor powders synthesized under different pH values: (a) pH=2 [5]; (b) pH=5 and (c) pH=8.

**3.2 Analysis of pH2 reduced powder**

In order to determine the particle morphology and phase structure of the reduced powder, the reduced pH2 powder was analyzed by HR-TEM. Fig 2 shows the HR-TEM images of the reduced powder reduced after 750℃ × 2 h + 900℃ × 4 h, followed by calcination at 550 ℃ for 4 h. Seen from Fig. 2a, the reduced powder presents a small spherical particle shape with regular morphology and good dispersion, and the particle size is about 40 nm, which is nanosized particles. The selected areas A and B correspond to Fig. 2b and (c, d), respectively. The reduced powder particles were calibrated with lattice fringes, as shown in Figs. 2(b-d). The measured spacing of lattice fringes are 0.2460 nm, 0.3227 nm and 0.3448 nm, respectively, which were close to the spacing of W (200), $ZrO_2$ (-111) and $Y_2O_3$ (202) crystal planes of PDF#47-1319, PDF#65-2357 and PDF#44-0399, respectively. As analysis above, the reduced pH2 powder is composed of tungsten and $ZrO_2$-$Y_2O_3$ nanosized particles.

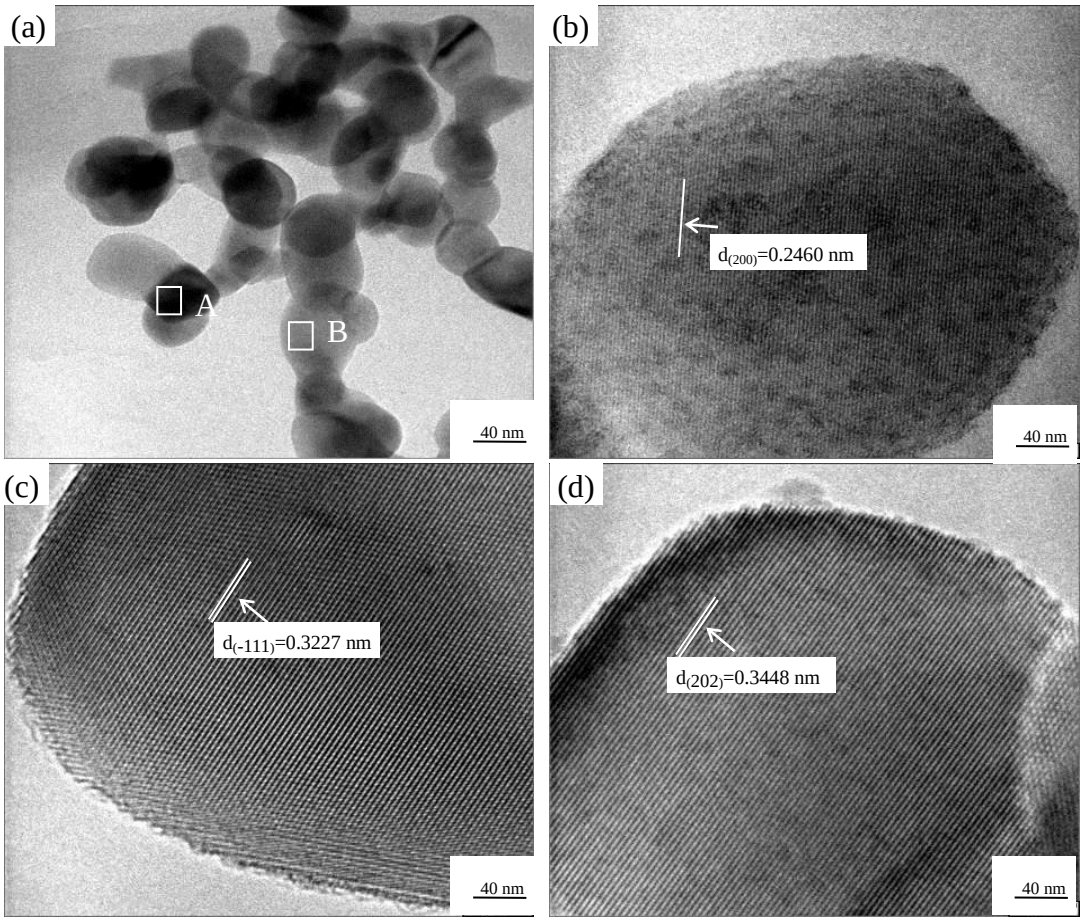


Fig.2 HR-TEM image and diffraction fringes of reduced powders: (a) HR-TEM image of reduced powders; (b) Diffraction fringes of W powder particle; (c) Diffraction fringes of $ZrO_2$ powder particle and (d) Diffraction fringes of $Y_2O_3$ powder particle.

It is concluded that the formation of $ZrO_2$-$Y_2O_3$ doped nanosized tungsten powder is related to the formation mechanism of doped tungsten powder at high temperature. During high temperature reduction, Y, Zr atoms always exists in the form of oxide, solid tungsten oxide would volatilize forming hydroxide $WO_2(OH)_2$ with high volatility. As the reduction reaction continues, hydroxide $WO_2(OH)_2$ would deposit on the surfaces of the neighbor tungsten oxide with low valence states or doped $Y_2O_3$-$ZrO_2$ particles [10]. The increase in growth rate and "volatilization-deposition" would make tungsten particles full growth in the reduction process [11]. However, the existence of $Y_2O_3$-$ZrO_2$

particles provide the plenty of crystal nucleus and then hinder the growth of tungsten particles, eventually forming the nanosized doped tungsten powder.

### 3.3 Microstructure and phase structure analysis of tungsten alloys

The BSE images of pure W and W-Zr(Y)$O_2$ alloys prepared under different pH values were shown in Fig. 3. Through EDS analysis, the black phase belongs to Zr(Y)$O_2$ particles consisting of three elements (Zr, Y, O) according to our previous researches [5, 7]. Seen from Figs. 4(a-c), it is obvious that there are lots of pores among alloys due to the pressureless sintering. In these alloys, the grains are almost same in size in range of 2-6 μm, much smaller than that of pure tungsten [6]. This is because of refinement effect of the Zr(Y)$O_2$ particles, most of which are almost located at W grain boundaries.

Detailed observation shows that there is difference in morphology and distribution of Zr(Y)$O_2$ among different W-$ZrO_2$ alloys. When alloy was prepared under pH value of 2, the Zr(Y)$O_2$ particles is smaller in size and distribute uniformly compared to other two alloys. There are few bonded particles observed. However, increasing pH value to 5, the occurrence of some obvious bonding $ZrO_2$ particles can be found marked by arrow A. When pH value increased to 8, there are more and more bonding particles observed, which are not conducive to the improvement of alloy properties.

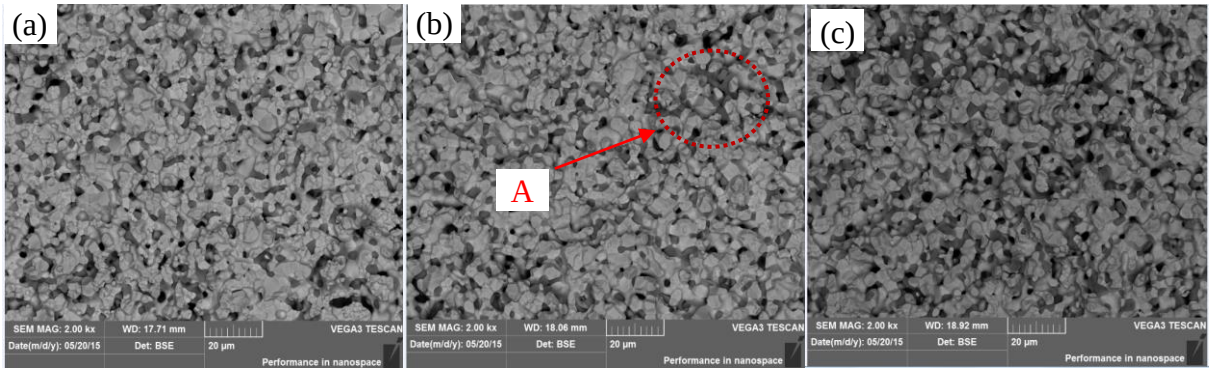


Fig.3 SEM images of W-Zr(Y)$O_2$ alloys: (a) pH2 alloy; (b) pH5 alloy; (c) pH8 alloy.

## 4. Mechanical properties of W-Zr(Y)$O_2$ alloy

### 4.1 Compressive properties of W-Zr(Y)$O_2$ alloy

The compressive properties of alloys prepared under different pH values of 2, 5 and 8 were compared as shown in Fig. 4a. The pH2 alloy has the highest compressive strength and failure strain compared with those of pH5 and pH8, respectively. The compressive strength and failure strain of pH2 alloy reaches to 1009 MPa and 0.22, respectively. With the increasing of pH value, the compressive strength decreases and the failure strain of the alloy becomes more and more worse.

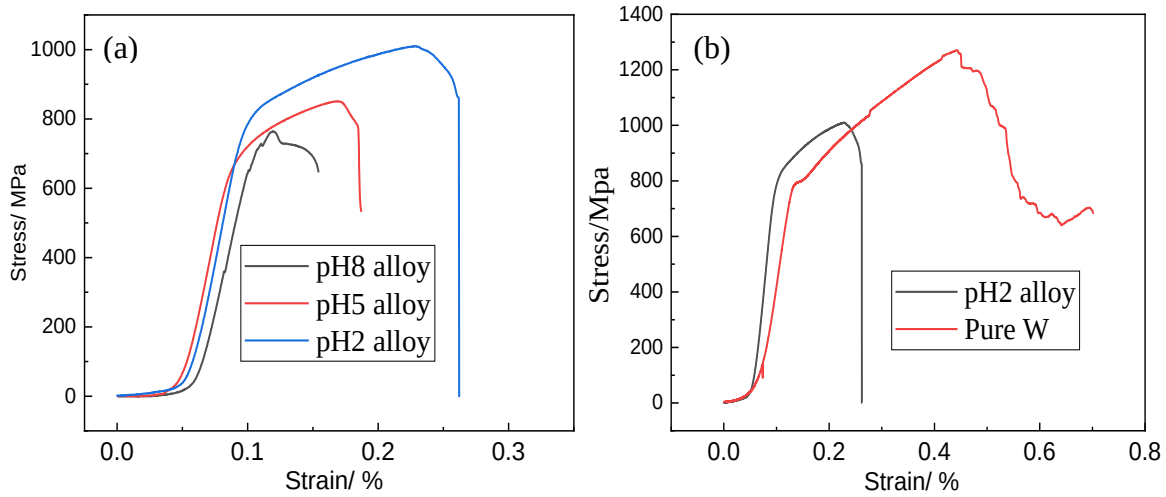

Fig.4 Compressive stress-strain curves of tungsten alloys: (a) Alloys prepared different pH values; (b) Pure W and W-Zr(Y)$O_2$ alloy.

As can be seen from Fig. 4b, the compressive strength of pH2 alloy reaches 1009MPa, 252MPa lower than that of the pure tungsten. This can be explained as follows: enrichment zone of oxide particles, caused by the high content of oxide particle, results in mutual superposition of stress field around the particles when the alloy is under loading. It leads to the fact that weakening effect on strength in alloy is greater than strengthening effect caused by dislocation motion, which weaken the bonding strength of the W-W grain boundaries and the fracture strain of W-Zr(Y)$O_2$ alloy.

### 4.2 Effect of Zr(Y)$O_2$ on wear resistance of tungsten alloy

As analysis above, the pH2 alloy possesses higher properties. Therefore, in this section, the effect of zirconia on wear resistance of pH2 alloy was investigated. Figs. 5(a, b) show the variation trend of the influence of abrasive particle and load on the wear properties of W-Zr(Y)$O_2$ alloy. As seen from Fig. 5a, the weight loss of alloy decreases with the decreasing of abrasive particles' size.

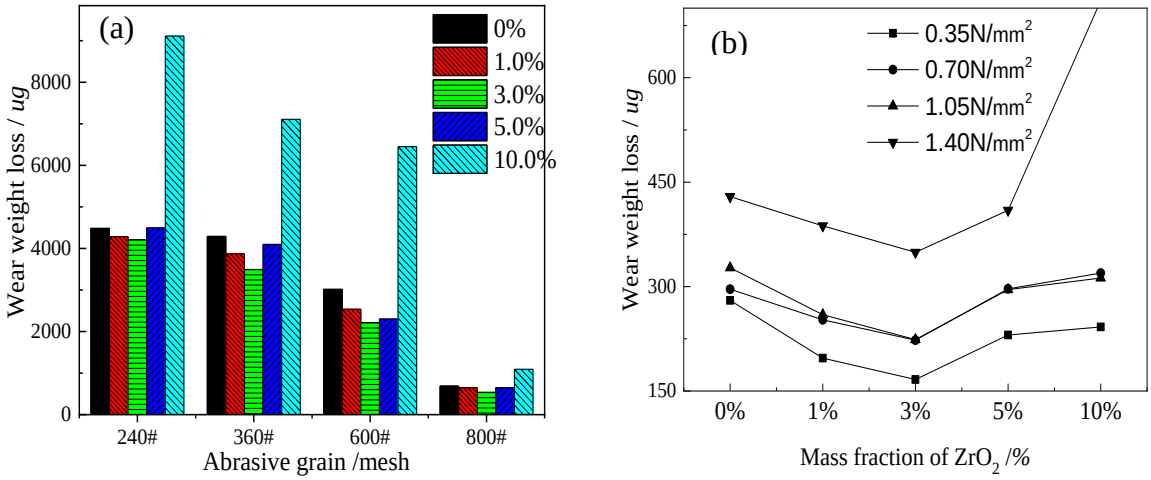


Fig. 5 Effect of abrasive particle and load on the wear weight loss of W-Zr(Y)$O_2$ alloys: (a) Abrasive particle; (b) Loading [6].

Under the same abrasive particles, the weight loss of W-Zr(Y)$O_2$ alloys shows a decreased trend with the increasing of $ZrO_2$ fraction to 3%, but with the further increasing of Zr(Y)$O_2$ fraction, the trend of weight loss increases. This variation trend was similar to our previous research [6], which shows the influence of load on the wear resistance of W-Zr(Y)$O_2$ alloy, as shown in Fig. 5b. It indicates that W-3.0%Zr(Y)$O_2$ alloy has the best wear resistance.

As the hardness of Zr(Y)$O_2$ particles is higher than that of the tungsten matrix, during wearing, the abrasive particles mainly interact with the Zr(Y)$O_2$ particles, so that the tungsten matrix is in a low wear zone, which reduces the wear loss of tungsten matrix. With the increase of zirconia content, there are more pores in alloys, which decrease the bonding strength between Zr(Y)$O_2$ and tungsten matrix. In the wear process, the abrasive particles firstly contact with the Zr(Y)$O_2$ particles, the higher load results in the Zr(Y)$O_2$ particles falling off from the matrix. As a result, the Zr(Y)$O_2$ particles and the abrasive particles ($Al_2O_3$) aggravate the wear of alloys together [12].

**Conclusion**

Different precursor powders were synthesized under different pH values of 2, 5 and 8. Morphologies of these precursor powders were compared, as well as the microstructures and properties of their corresponding alloys. That precursor powder synthesized under solution with pH=2

possesses finer particles structure. W-Zr(Y)$O_2$ alloy prepared under pH=2 possesses better microstructure and compressive properties compared to other two alloys prepared under pH=5, 8, respectively. The effect of Zr(Y)$O_2$ mass fraction on the abrasion resistance of tungsten alloy were investigated. Mechanical properties of W-Zr(Y)$O_2$ alloy prepared under pH=2, as well as abrasion resistance, were compared to pure tungsten.

**References**


[1] M. Kawai, M. Furusaka, K. Kikuchi, H. Kurishita, R.Watanabe, J. F. Li, K. Sugimoto, T. Yamamura, Y. Hiraoka, K. Abe, A. Hasegawa, M. Yoshiie, H. Takenaka, K. Mishima, Y. Kiyanagi, T. Tanabe, N. Yoshida, T. Igarashi, R&D of a MW-class solid-target for a spallation neutron source, J. Nucl. Mater. 318 (2003) 38-55.

[2] L. J. Xu, F. N. Xiao, S. Z. Wei, Y. C. Zhou, K. M. Pan, X. Q. Li, J. W Li, W. L, Development of tungsten heavy alloy reinforced by cubic zirconia through liquid-liquid doping and mechanical alloying methods, Int. J. Refract. Met. Hard Mater. 78 (2019) 1-8.

[3] L. Veleva, R. Schaeublin, M. Battabyal, T. Plociski, N. Baluc, Investigation of microstructure and mechanical properties of W-Y and W-$Y_2O_3$ materials fabricated by powder metallurgy method, Int. J. Refract. Met. Hard Mater. 50 (2015) 210-6.

[4] P. K. Senapati, B. K. Mishra, A. Parida, Modeling of viscosity for power plant ash slurry at higher concentrations: effect of solids volume fraction, particle size and hydrodynamic interactions, Powder Technol. 197, 2010, 1–8. https://doi.org/10.1016/j.powtec.2009.07.005

[5] F. Xiao, L. Xu, Y. Zhou, K. Pan, J. Li, W. Liu, S. Wei, A hybrid microstructure design strategy achieving W-$ZrO_2$(Y) alloy with high compressive strength and critical failure strain, J Alloy Compd. 708 (2017) 202-212.

[6] F. N. Xiao, L. J. Xu, Y. C. Zhou, K. M. Pan, J. W. Li, W. Liu, S. Z. Wei, Preparation, microstructure, and properties of tungsten alloys reinforced by $ZrO_2$ particles, Int. J. Refract. Met. Hard Mater. 64 (2017) 40-46.

[7] F. N. Xiao, Q. Miao, S. Z. Wei, T. Barriere, G. Cheng, S. W. Zuo, L. J. Xu, Uniform nanosized oxide particles dispersion strengthened tungsten alloy fabricated involving hydrothermal method and hot isostatic pressing, J Alloys Compd, 824 (2020): 153894..

[8] F. N. Xiao, Q. Miao, S. Z. Wei, Z. Li, T. L. Sun, L. J. Xu, Microstructure and mechanical properties of W-$ZrO_2$ alloys by different preparation techniques, J Alloys Compd, 774 (2019): 210-221.

[9] L. J. Xu, S. Z Wei, Q. Liu, G. S Zhang, J. W. Li, Microstructure and High-Temperature Frictional Wear Property of Mo-Based Composites Reinforced by Aluminum and Lanthanum Oxides, Tribology Transactions, 56 (2013): 833-840.

[10] F. N. Xiao, Q. Miao, S. Z. Wei, Hydrothermal synthesis of nanoplates assembled hierarchical h-$WO_3$ microspheres and phase evolution in preparing cubic Zr (Y) $O_2$-doped tungsten powders, Adv. Powder Technol. 29 (2018) 2633-2643.

[11] P. Lu, C. Y. Shen, T. Qiu. Preparation of sub-micron tungsten powder doped with CeO2[J]. Powder Metallurgy Industry, 2008, 18(2): 6-8.

[12] S. Z. Wei, L. J. Xu, Review on Research Progress of Steel and Iron Wear-Resistant Materials. Acta Metall Sin, 2020, 56(4): 523-538.